STUDIUM GRADIENTŮ ZBYTKOVÝCH NAPĚTÍ A MIKROTVRDOSTI V POVRCHOVÝCH VRSTVÁCH LEŠTĚNÝCH VZORKŮ OCELÍ

STUDY OF RESIDUAL STRESS AND MICROHARDNESS GRADIENTS IN SURFACE LAYERS OF POLISHED STEEL SAMPLES

Nikolaj GANEV, Marian ČERŇANSKÝ, Petr BOHÁČ, Václav NOVÁK, Jan DRAHOKOUPIL, Radim ČTVRTLÍK, Martin STRANYÁNEK[1]

Abstrakt

Příspěvek obsahuje výsledky rtg difrakční analýzy gradientů zbytkových makroskopických a mikroskopických napětí v povrchových vrstvách leštěných vzorků pěti typu ocelí (ČSN 12050, 14220, 17135, 19313, 19852) odlišného chemického složení. Mechanické vlastnosti materiálů ve výchozím stavu byly stanoveny tahovou zkouškou. Studované povrchy byly rovněž charakterizovány pomocí nanoindentace. Cílem práce bylo najít a formulovat dílčí korelace mezi stavem deformace krystalové mřížky povrchu generovaného tímto technicky významným finálním opracováním, jeho mikrotvrdostí a pevnostními charakteristikami výchozích materiálů.

Klíčová slova: oceli, leštění, makroskopická a mikroskopická zbytková napětí, mechanické vlastnosti, nanoindentace, mikrotvrdost.

Abstract

The contribution presents the results of X-ray diffraction analysis of both the macroscopic and microscopic residual stresses (RS) in burnished surface layers of five different steels (ČSN 12050, 14220, 17135, 19313, 19852). Mechanical properties of as-received materials were obtained by tensile tests. The instrumented nanoindentation testing was applied for surface characterization as well. The main goal of the investigations was to find correlations between the lattice deformation of the studied surfaces, their microhardness and mechanical properties.

Keywords: steels, burnishing, macroscopic and microscopic residual stresses, mechanical properties, nanoindentation, microhardness.

INTRODUCTION

Residual stresses represent one of the most important attributes of surface layers. Under elastic-plastic deformation, individual crystallites are differently deformed and this gives rise to microscopic internal stresses, which are accompanied by macroscopic stresses [1, 2]. Although the mutual action of both types of residual stresses is inevitable, their acting concurrently is not systematically studied. X-ray diffraction analysis is a reliable method for non-destructive obtaining this information, in thin layers beneath surface within the penetration depth of used radiation.

Burnishing is an important technique of finishing leading to brilliant gloss that increases the surface quality, so it is necessary, e.g. prior to surface deposition of metals, or in order to reduce the coefficient of friction, etc.

[1] doc. Ing. Nikolaj GANEV, CSc., KIPL, FJFI ČVUT v Praze, ganev@troja.fjfi.cvut.cz
Lektoroval doc. Ing. Jozef BOCKO, CSc., KAMaM, SjF TU v Košiciach, jozef.bocko@tuke.sk

SAMPLES UNDER INVESTIGATION

Five *Fe* alloys were used to prepare a set of analysed samples 50 × 50 × 5 mm^3 in size, namely: carbon ferrite steel ČSN 12 050 (A), *Mn-Cr* steel 14 220 (B), *Cr-Mo* corrosion-resistant steel 17 135 (C), low-alloyed tool steel 19 313 (D), and *Mo-W-Co* rapid steel 19 852 (E) (Table 1). Prior to grinding the samples were annealed (stress-relieved) in *Ar* for 2 hours at 550 °C. Thereafter the samples were burnished to specular gloss with various diamond pastes.

Chemical composition of the investigated materials Table 1

Steel	Content, % weight			
	C	*Mn*	*Mo*	*Cr*
A	0.42 – 0.5	0.5 – 0.8	–	0 – 0.25
B	0.14 – 0.19	1.1 – 1.4	–	0.8 – 1.1
C	0.17 – 0.23	0.5 – 1	0.8 – 1.2	10 – 12.5
D	0.8 – 0.9	1.75 – 2.1	–	0.2 – 0.4
E	0.8 – 0.9	0 – 0.45	4.5 – 5.5	3.8 – 4.6

Flat specimens of thickness 2 mm (see Fig.1) were made for tensile tests from materials above and then annealed in the same way.

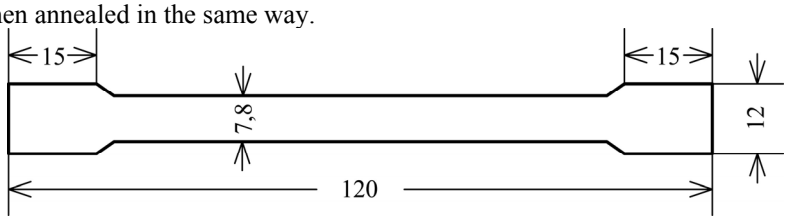

Fig. 1 Form of the specimens made for tensile tests. Dimensions are in millimetres.

EXPERIMENTAL PROCEDURES APPLIED

The average lattice strain $\bar{\varepsilon}_\psi$ within the effective depth T^e of penetration of used radiation measured in the direction of the normal N^{hkl} to diffracting planes (hkl) can be expressed for symmetrical state of residual macroscopic stresses $(\sigma_{11} = \sigma_{22})$ by the relation [1]

$$\bar{\varepsilon}_\psi = \tfrac{1}{2}s_2(\bar{\sigma}_{11} - \bar{\sigma}_{33})\sin^2\psi + \tfrac{1}{2}s_2\bar{\sigma}_{33} + s_1(2\bar{\sigma}_{11} + \bar{\sigma}_{33}), \qquad (1)$$

where $\bar{\sigma}_{11}$, $\bar{\sigma}_{22}$ are mean values of the stress tensor components and ½s$_2$, s$_1$ are X-ray elastic constants. If the quantities σ_{11}, σ_{22} vary linearly with the distance T from the surface within the effective depth T^e of penetration, i.e.,

$$\bar{\sigma}_{11} = \sigma_{11}(0) + g_{11}T^e, \qquad \sigma_{33} = g_{33}T^e,$$

than the relation (1) can be written as

$$\bar{\varepsilon}_\psi = \tfrac{1}{2}s_2(\sigma_{11}(0) + g_{11}T^e - g_{33}T^e)\sin^2\psi + \tfrac{1}{2}s_2g_{33}T^e + s_1(2\sigma_{11}(0) + 2g_{11}T^e + g_{33}T^e), \qquad (2)$$

where $\sigma_{11}(0)$, g_{11}, g_{33} are unknown quantities, $\bar{\varepsilon}_\psi$ - experimental values, and T^e have to be calculated for the corresponding angles ψ. If at least three values of $\bar{\varepsilon}_\psi$ are measured, the quantities $\sigma_{11}(0)$, g_{11}, g_{33} can be obtained from eq. (2) by a fitting procedure.

Single line Voigt function method [3] was used for calculations of microstrains and particle (grain, crystallite) size.

The single line Voigt function method is based on the assumptions that the particle size leads to the Cauchy (Lorentz) profile and the microstrain is connected with the Gauss profile. The additional assumption is, that both these factors are composed independently. Mathematically it means, that the physical diffraction profile is a convolution of Cauchy and Gauss profiles, which is the Voigt function. The most important quantity is the shape factor φ of a diffraction line, which is defined as the ratio of the full width $2w$ at the half of the maximum (FWHM) to the integral breadth of the line β, *i.e.* $\varphi = 2w/\beta$.

The Cauchyian and the Gaussian part of the integral width of the Voigt function is given by the following relations

$$\beta_C = \beta\,(2.0207 - 0.4803\,\varphi - 1.7756\,\varphi^2) \tag{3}$$

$$\beta_G = \beta\,(0.6420 + 1.4187\,(\varphi - \varphi_C)^{1/2} - 2.2043\,\varphi + 1.8706\,\varphi^2), \tag{4}$$

where $\varphi_C = 2/\pi = 0.6366$ is the shape factor of the Cauchy function (the shape factor of the Gauss function is $\varphi_G = 2\,((\ln 2)/\pi)^{1/2} = 0.9394$). The maximal error of the relations (3) and (4) is approximately 1 %.

Relations (3) and (4) are used to decompose the integral width of a measured diffraction profile h on the Cauchyian part β_C^h and Gaussian part β_G^h. The same procedures are used for the instrumental profile g, which is obtained from a measurement on a convenient standard, without a diffraction (physical) broadening. The Cauchyian β_C^g and Gaussian β_G^g parts of the instrumental profile are estimated also from the relations (3) and (4).

The Cauchyian β_C^f and the Gaussian β_G^f parts of the integral width of the physical profile f are determined from relations

$$\beta_C^f = \beta_C^h - \beta_C^g \tag{5}$$

$$(\beta_G^f)^2 = (\beta_G^h)^2 - (\beta_G^g)^2\,. \tag{6}$$

The particle size D and the microstrain ε are given by the relations

$$D = \lambda / (\beta_C^f \cos\theta) \tag{7}$$

$$\varepsilon = \beta_G^f / (4\,\mathrm{tg}\,\theta), \tag{8}$$

where λ is the wave length and θ is Bragg angle.

Nanoindentation is an important and effective experimental method. The instrumented nanoindentation testing provides a common method for measuring mechanical properties of materials on small scales. The indentations were carried out in the low load range of the Micro Materials platform NanoTest 600. A three-faced pyramidal Berkovich diamond indenter with semi-apical angle 65.3° and tip radius ~ 100 nm was used. The force-displacement raw data recorded in each test during depth sensing indentation (DSI) were first processed with a deduction of the previously calibrated machine compliance to get the "net" data.

A typical curve from DSI data is in Fig.2. It consists of three parts: loading, unloading and creep during dwell time at maximal load F_{max}; h_{max} is corresponding indentation depth. h_f then corresponds final depth when during unloading the force F drops to F = 0. It roughly expresses depth of residual impression which size on surface is optically measured to evaluate quantity of hardness in the traditional sense.

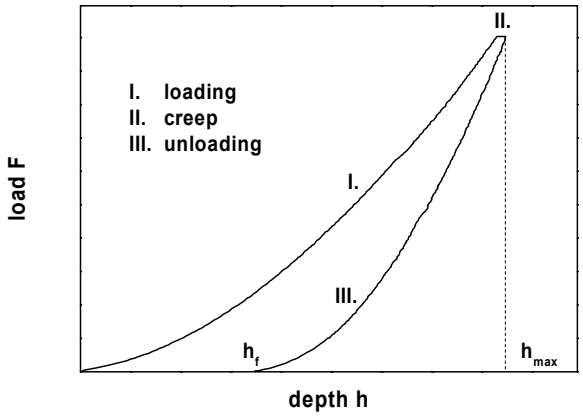

Fig. 2 A typical curve obtained from nanoindentation consists of parts I. – III. The definitions of indentation depths h_{max} and h_f

A revised linear analytical method was used in deriving unloading compliance C_S and contact depth h_C values, in which 60 % of the unloading data was used for a power law curve fitting. Since the diamond area function (which defines the relation of indent projected area A_C and contact depth, h_C) has been independently calibrated as

$$A_C = k_1(h_C)^2 + k_2 h_C , \tag{9}$$

the following equations can be used in calculating hardness H and Young's modulus E values of the test samples:

$$H = F_{max} / A_C \tag{10}$$

$$E_r = \sqrt{\pi} / [2 C_S \sqrt{A_C}] \tag{11}$$

$$1 / E_r = [1 - (\nu_i)^2] / E_i + [1 - \nu^2] / E, \tag{12}$$

where E_r is reduced modulus, an intermediate parameter for the non-rigid inter-specimen contact effect. E_i and ν_i are Young's modulus and Poisson's ratio for the (diamond) indenter, which can be taken as 1140 GPa and 0.07, respectively. E and ν are then Young's modulus and Poisson's ratio for the test sample [4].

MEASUREMENT CONDITIONS

X-ray diffraction stress analysis was performed on an ω-goniometer Siemens with *CrKα* radiation. Macroscopic and microscopic lattice strains were evaluated from the *α-Fe {211}* diffraction line detected for nine tilt angles ψ ($sin^2\psi$ = 0, 0.1, 0.2, …, 0.8). In stress calculations the X-ray elastic constants $½s_2 = 5.76 \cdot 10^{-6}$ MPa^{-1}, $-s_1 = 1.25 \cdot 10^{-6}$ MPa^{-1} were used. Unstressed lattice parameters for each material were determined from the stress-relieved samples.

Analyses were performed on a *NanoTest™ NT600* measuring system equipped with a Berkovich indenter. All the samples were investigated with a load of 50 mN being used four times. Experiments were evaluated according to Oliver-Pharr method [5] (in software package). It is based on the fitting of second-order polynomial expressions to the unloading curves at their beginning. Then the contact stiffness S and compliance C are defined by means of derivation of fitted polynomial as

$$S = dF / dh = 1 / C. \tag{13}$$

The hardness H is calculated according to formula (10) and reduced modulus E_r by substitution of formula (13) into (11). Moreover, if investigated material has considerable less elastic modulus then diamond the first fraction in the right hand side equation (4) is negligible against the second and the formula simples to

$$E^* \sim E_r = E / [1 - \nu^2]. \quad (14)$$

Tensile tests were performed at room temperature in an INSTRON 1195 testing machine at strain rate $4 \cdot 10^{-3}$ s^{-1}.

RESULTS AND THEIR DISCUSSION

The centrally symmetric state of macroscopic residual stresses was found in the surface layers of studied samples. Since the obtained courses of lattice deformation ε vs. $sin^2\psi$ are not linear (see Fig. 2), the stress fields are non-uniform within the penetration depth of used radiation. The experimental error represents the least squares standard deviation

The macroscopic surface stresses $\sigma(0)_\varphi$ are compressive with positive gradients from 26 to 40 MPa·μm^{-1} except of the higher values obtained for the steel C (see Table 2).

Microscopic stresses σ_{micro} are also inhomogeneous (Table 2), the surface values (for $sin^2\psi$ = 0.7 – 0.8) are higher than those in the depth ($sin^2\psi$ = 0.1 – 0.2). The standard least squares deviation is approximately 3 %.

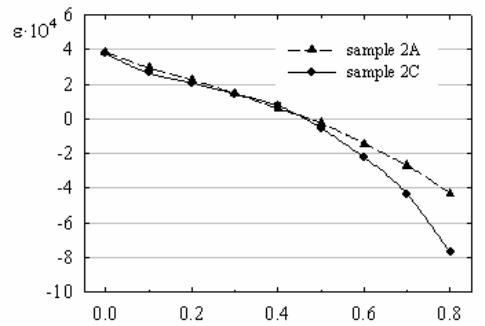

Fig.3 Experimental distributions of lattice deformation ε vs. $sin^2\psi$ obtained for the sample 2A (g_φ= 25,6 MPa·μm^{-1}) and 2C (g_φ = 70,6 MPa·μm^{-1})

Surface residual stresses $\sigma(0)_\varphi$, their gradients g_φ, and the gradient g_3 of the normal stress σ_3. The surface value is $\sigma_3(0)$ = 0. The experimental error represents the least squares standard deviation **Table 1**

Sample	$\sigma(0)_\varphi$, MPa	g_φ, MPa·μm^{-1}	g_3, MPa·μm^{-1}
1A	– 244,9 ± 19,8	32,7 ± 6,2	4, 1± 1,4
2A	– 251,6 ± 9,6	25,6 ± 3,0	3,7 ± 0,7
1B	– 214,8 ± 18,5	31,1 ± 5,8	5,3 ± 1,3
2B	– 245,3 ± 20,4	34,1 ± 6,4	3,9 ± 1,4
1C	– 367,2 ± 22,0	56,3 ± 7,0	0,1 ± 1,6
2C	– 490,4 ± 30,8	70,6 ± 9,8	2,8 ± 2,3
1D	– 364,7 ± 13,9	39,6 ± 4,4	0,8 ± 1,0
2D	– 404,9 ± 13,2	36,7 ± 4,2	– 0,6 ± 1,0
1E	– 618,7 ± 13,8	26,0 ± 4,4	–25,2 ± 1,0
2E	– 561,7 ± 19,3	29,2 ± 6,1	– 22,8 ± 1,4

Microstrains $\varepsilon_{micro} \cdot 10^{-4}$ for tilt angles ψ ($sin^2\psi$) obtained from the analyzed samples **Table 2**

$\sin^2\psi$	0.0	0.1	0.2	0.3	0.4	0.5	0.6	0.7	0.8
1A	5.0	4.7	4.5	4.3	4.2	4.4	4.5	5.1	5.2
2A	5.0	4.9	4.7	4.6	4.5	4.7	4.8	5.1	4.6
1B	4.6	4.0	3.6	3.4	3.2	3.4	3.7	4.3	4.8
2B	5.1	4.5	4.2	3.8	3.8	3.8	4.1	4.7	5.3
1C	8.3	7.9	7.9	7.8	7.8	7.7	8.6	9.6	12.3
2C	9.3	9.0	8.9	8.6	8.6	9.0	9.9	11.1	12.2
1D	6.6	5.9	5.4	4.9	5.0	5.1	5.4	6.3	6.4
2D	7.0	6.0	5.4	4.8	4.7	4.8	5.3	6.1	6.3
1E	8.6	8.4	8.4	8.4	8.8	9.0	9.5	9.8	10.7
2E	7.9	7.4	7.1	6.9	6.9	7.3	7.7	8.1	9.0

Indentation hardness, reduced modulus and their standard deviations measured on the burnished steel samples under the load of 50 mN **Table 3**

Sample	Max. depth st. dev. [nm]	Plastic depth st. dev. [nm]	Hardness st. dev. [GPa]	Red. modulus st. dev. [GPa]
1A	946 ± 89	912 ± 89	2.5 ± 0.46	225 ± 36
2A	960 ± 176	930 ± 187	2.56 ± 0.95	258 ± 51
1B	1073 ± 32	1042 ± 33	1.89 ± 0.12	209 ± 8
2B	1048 ± 4	1014 ± 5	1.99 ± 0.02	196 ± 13
1C	741 ± 19	698 ± 21	4.1 ± 0.24	220 ± 7
2C	727 ± 19	686 ± 20	4.25 ± 0.24	233 ± 16
1D	880 ± 16	845 ± 12	2.84 ± 0.08	233 ± 33
2D	868 ± 49	824 ± 51	3 ± 0.34	185 ± 7
1E	748 ± 6	709 ± 7	3.98 ± 0.08	237 ± 4
2E	794 ± 27	761 ± 33	3.48 ± 0.3	267 ± 41

Mechanical properties of studied materials **Table 4**

Alloy	Yield stress, R_p, MPa	Tensile strength, R_m, MPa	Max. elongation ε_{max}
A	381	817	0,264
B	269	585	0,288
C	1007	1232	0,113
D	386	786	0,247
E	437	947	0,190

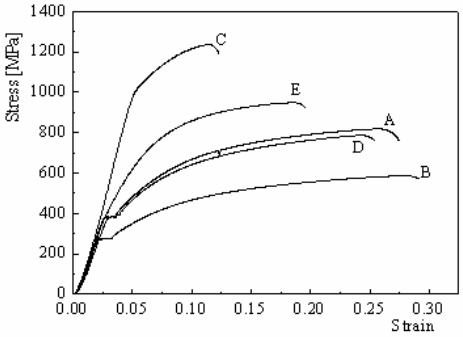

Fig. 4 The results of tensile tests on the five steels under investigation.

CONCLUSIONS

- A pronounced relationship between the characteristics $|\sigma\varphi|$, σ_{micro}, H, R_p, R_m and ε_{max} depicted in Fig. 5 is evident.
- The courses in Fig. 5 are analogous with a strong correlation between surface microscopic stresses and hardness.
- The results obtained in the initial stage of a parallel X-ray diffraction macro- and micro- stress analysis and nanoindentation examinations are promising.
- Specifying correlations between depth profiles of the observed quantities needs a detailed study.

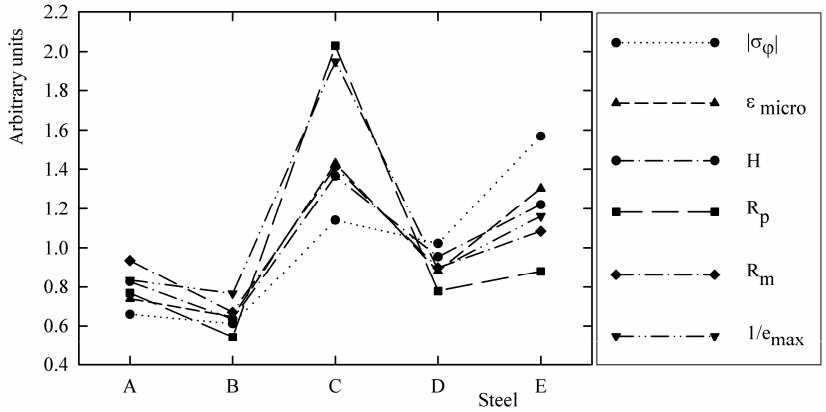

Fig. 5 The absolute values of surface compressive macroscopic stresses $|\sigma\varphi|$, microstrains ε_{micro}, the hardness H in the depth, yield stress R_p, tensile strength R_m, and maximal elongation e_{max} obtained for the investigated materials normed to the average value of each quantity for all the materials investigated

The research was supported by the Project № 101/05/2523 of the Czech Science Foundation and by the Nat. Res. Projects AV0Z10100520, AV0Z10100522 of the Czech Republic.

REFERENCES

[1] I. KRAUS, N. GANEV: *Residual Stress and Stress Gradients*, In: Industrial Applications of X-ray Diffraction, Eds. F.H.Chung and D.K.Smith, Marcel Dekker, Inc., New York-Basel, 2000, pp. 793-8112.
[2] R. DELHEZ, Th.H. de KEIJSER, E.J. MITTEMIJER, *Surface Engineering* 3, 1987, 331-342.
[3] Th.H. de KEIJSER, J.I. LANGFORD, E.J. MITTEMEIJER, A.B.P. VOGELS, J. *Appl. Cryst.* 15, 1978, 308-314.
[4] B. BEAKE, S. GOODES, S. JONES, R. PARKINSON, N. PICKFORD, J. SMITH: *Micro Materials NanoTest User Manual*, ver. 2.0, Micro Materials Ltd., UK, 2003.
[5] W.C. OLIVER, G.M. PHARR, *J. Mater. Res*. 7, 1992, 1564.